Inorganic Chemistry

Article

pubs.acs.org/IC

Size-Controlled Synthesis of Ag Nanoparticles Functionalized by Heteroleptic Dipyrrinato Complexes Having *meso*-Pyridyl Substituents and Their Catalytic Applications

Rakesh Kumar Gupta,[†] Mrigendra Dubey,[†] Pei Zhou Li,[‡] Qiang Xu,[‡] and Daya Shankar Pandey*[,†]

[†]Department of Chemistry, Faculty of Science, Banaras Hindu University, Varanasi 221 005 (U.P.), India

[‡]National Institute of Advanced Industrial Science and Technology, 1-8-31, Midorigaoka, Ikeda, Osaka 563-8577, Japan

Supporting Information

ABSTRACT: The syntheses of heteroleptic dipyrrinato nickel(II) complexes [Ni(4-pydpm)(dedtc)] (**1**) and [Ni(4-pydpm)(dipdtc)] (**2**) [4-pydpm = 5-(4-pyridyl)dipyrromethene; dedtc = diethyldithiocarabamate; and dipdtc = diisopropyldithiocarbamate] and the thorough characterization of these complexes by satisfactory elemental analyses, electrospray ionization mass spectrometry, Fourier-transform infrared, NMR (^{1}H, ^{13}C), and UV−vis spectroscopies, and electrochemical studies was achieved. Structure of **1** was authenticated by X-ray single-crystal analysis. Both the complexes **1** and **2** were successfully utilized as a capping agent in the preparation of silver nanoparticles. Availability of free pyridyl nitrogen on the dipyrrin core of these complexes was meticulously exploited in functionalization and stabilization of the silver nanoparticles (AgNPs). Morphological and structural investigations on colloidal nanoparticles were followed by UV−vis spectroscopy and transmission electron microscopy (TEM). Overall results revealed that average size of the silver nanoparticles (~10, 15, 20 nm, and aggregation) is strongly influenced by ratio of Ag/[**1**/**2**] (03, 06, 10, 20). Correlation between particle size and capping agents was realized by UV−vis and TEM studies. Catalytic activity of the AgNPs obtained through this route was successfully employed in the reduction of 4-nitrophenol (4-NP) to 4-aminophenol (4-AP). It was established that reduction process follows a pseudo-first-order kinetics.

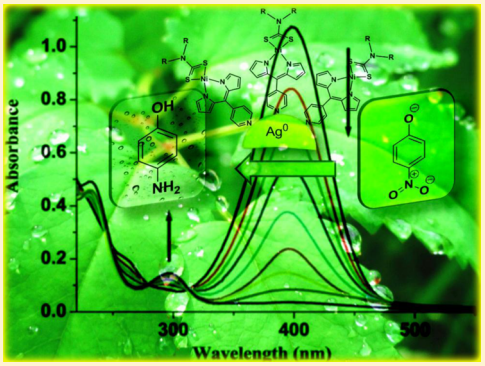

INTRODUCTION

Metallic nanocomposite materials, particularly those based on platinum, silver, and gold, have attracted a great deal of attention during recent years due to their interesting photophysical properties, small particle size, and surface plasmon behavior.[1] In this context, synthesis of the functionalized silver nanoparticles (AgNPs) and its application in diverse areas have drawn special attention.[2] It has been established that the shape, size, and size distribution of AgNPs strongly depends on several factors, namely, reaction conditions, temperature, reaction time, pH of the reaction medium, solvents employed, molar ratio of the silver(I) nitrate, reducing and capping agents, etc.[3] Moreover, because of their effective activity against a broad spectrum of microorganisms including bacteria, yeast, and fungi, these are also employed in medicine, treatment of burn injuries, and various infections.[4] In addition, these are indispensable in many organic transformations.[5] It is well-known that 4-nitrophenol (4-NP) presents one of the most notorious toxic pollutants in the industrial effluents. On the other hand, closely related amino derivative 4-aminophenol (4-AP) is of great importance in pharmaceuticals and dye industries and is used as a photographic developer, corrosion inhibitor, and hair-dyeing agent.[6] Therefore, immense current interests have arisen in the development of catalysts/agents for reduction of the 4-NP to 4-AP.[5] Traditional methods for the said process usually involve multistep iron/acid, reduction/catalytic hydrogenation.[7] Considering these aspects, size-controlled synthesis of AgNPs for organic transformations in a simple, cost-effective, and selective manner is highly demanding.[8]

All together, dipyrromethenes (dipyrrins) are highly conjugated bispyrrollic systems, which behave as monoanionic bis-chelating ligand and form a variety of compounds ranging from BODIPYs to homo/heteroleptic complexes.[9] These exhibit rich optical properties and find potential application in diverse areas.[9] The incorporation of a pyridyl/imidazolyl moiety in the dipyrrin core leads to the creation of attractive architectures and topologies with various metal ions, particularly, silver salts.[10] At the same time, nickel is an important transition metal, which under suitable conditions form nickel nanoparticles (NiNPs). Notably, nickel-based nanoparticles have recently been utilized as efficient catalysts in the hydrogenation of nitrobenzene, nitrophenol, reduction of oxygen, and oxidation of olefins.[11] Simultaneously, dithiocarbamates have been extensively used in the fabrication of optical

Received: June 27, 2014
Published: February 20, 2015

DOI: 10.1021/ic502848a
Inorg. Chem. 2015, 54, 2500−2511

and semiconducting devices, systems of biological significance, nanoparticle synthesis, etc.[12] In their seminal work Mayer et al. have reported gold or silver nanocomposites functionalized by inorganic complexes based on polyoxometalate,[13a] thiometalate,[13b,c] 1,10-phenanthroline,[13d,e] and pyridyl groups.[13d,f,g] Although, numerous reports dealing with the application of the conventional thiol group in synthesis of AgNPs have been described, those involving pyridyl nitrogen are rather scarce.[13,14] It was realized that incorporation of the *meso* substituents having a pyridyl group on the dipyrrin core may offer a promising and good choice for the functionalization and stabilization of AgNPs in colloidal solution. With an objective of developing new compounds having potential to act as a good capping agent for AgNPs two new nickel complexes possessing both dithiocarbamate and pyridyl functionalities were designed and synthesized.

With this contribution, syntheses and thorough characterizations of **1** and **2** together with their efficacy as a capping agent for the synthesis of AgNPs are described. Further, catalytic efficiency of the AgNPs for transformation of 4-NP to 4-AP are also reported. To the best of our knowledge this is the first report dealing with functionalization and catalytic activity of AgNPs by metal dipyrrinato complexes.

EXPERIMENTAL SECTION

Reagents. All the reactions were performed in deaerated solvents under nitrogen atmosphere. The solvents were purified following literature procedure prior to its use.[15] Diethyl-/diisopropyl amine, carbon disulfide, 2,3-dichloro-5,6-dicyano-1,4-benzoquinone (DDQ), 4-pyridinecarbaldehyde, benzaldehyde, acetylacetone, poly(vinylpyrrolidone) (PVP, average molecular weight ≈ 55 000), sodium borohydride ($NaBH_4$), 4-nitrophenol, pyrrole, silver(I)-nitrate, and nickel(II) chloride hydrate were procured from Sigma-Aldrich Chemical Co., USA, and used as received without further purifications. The precursor complexes $[Ni(dtc)_2]$ (dtc = diethyldithiocarabamate (dedtc), diisopropyldithiocarbamate (dipdtc)) and 5-(4-pyridyl)-dipyrromethane (4-pydpmH) were synthesized and purified by literature procedures.[16]

General Methods. Elemental analyses for carbon, hydrogen, and nitrogen were performed on an Exeter Analytical Inc. model CE-440 CHN analyzer. IR and UV−vis spectra were acquired on a Varian 3300 FT-IR, and Shimadzu UV-1601 spectrophotometers, respectively. ^1H (300 MHz) and ^{13}C (75.45 MHz) NMR spectra were obtained on a JEOL AL300 FT-NMR spectrometer using tetramethylsilane $[Si(CH_3)_4]$ as an internal reference. Electrospray ionization mass spectrometric (ESI-MS) measurements were made on a THERMO Finningan LCQ Advantage Max ion trap mass spectrometer. In a typical measurement, samples (10 μL) were dissolved in dichloromethane/acetonitrile (3:7, v/v) and introduced into the ESI source through a Finningan surveyor auto sampler. Mobile phase (MeOH/MeCN/H_2O, 90:10) flowed at a rate of 250 μL/min. Ion spray and capillary voltage were set at 5.3 kV and 34 V, respectively. The MS scans were run up to 2.5 min, and spectra print-outs are averages of more than 10 scans. Electrochemical measurements were made on a CHI 620c electrochemical analyzer. All the measurements were made in a single compartment cell equipped with a glassy carbon working, platinum wire counter, and Ag/Ag^+ reference electrode under nitrogen atmosphere. Transmission electron microscopy (TEM) and high-resolution (HR) TEM images were captured on HR TEM (JEOL JEM 2100) and an Ultra Modern Transmission Electron Microscope (FEI). The samples were loaded over lacy carbon-coated copper TEM grids (300 mesh) were dried under ambient conditions and imaged at accelerating voltage of 200 and 120 kV, respectively. Elemental mapping on the samples was performed using in situ energy-dispersive X-ray scanning transmission electron microscopy (EDX-STEM, Oxford Instrument Inc., INCA X-sight).

Synthesis of [Ni(4-pydpm)(dedtc)] (1). DDQ (0.114 g, 0.50 mmol) dissolved in benzene (20 mL) was added dropwise with stirring to an ice-cooled stirring solution of 4-pydpmH (0.112 g, 0.50 mmol, dichloromethane, 30 mL), and the reaction mixture was stirred for an additional 1 h at room temperature (rt). After filtration, it was concentrated to dryness under reduced pressure to afford a red-brown solid. Resulting mass thus obtained was dissolved in dichloromethane (40 mL) and filtered to remove any solid impurities. Triethylamine (1 mL) and precursor complex $[Ni(dedtc)_2]$ (0.182 g, 0.50 mmol) were successively added to the filtrate, and the resulting reaction mixture stirred overnight at rt. It was concentrated to dryness under reduced pressure, and the ensuing product was purified by column chromatography (SiO_2; CH_2Cl_2/hexane, 60:40) to afford a dark red solid. Yield: (0.074 g; 35%). Anal. Calcd for $C_{19}H_{20}N_4NiS_2$: C, 53.42; H, 4.72; N 13.11. Found: C, 53.53; H, 4.65; N, 13.02%. ^1H NMR ($CDCl_3$, δ_H ppm): 8.68 (s, 2H, pyridyl), 7.36 (d, 2H, J = 39 Hz, pyridyl), 7.03 (s, 2H, J = 39 Hz, pyrrole), 6.47 (d, 2H, J = 36 Hz, pyrrole), 6.27 (d, 2H, J = 36 Hz, pyrrole), 3.64 (q, 4H, $C\underline{H}_2CH_3$), 1.27 (t, 6H, $CH_2C\underline{H}_3$). ^{13}C NMR ($CDCl_3$, δ_C ppm): 202.08, 150.65, 148.83, 145.62, 142.29, 134.37, 131.51, 124.99, 118.17, 44.40, 12.39. ESI-MS. Calcd, found: m/z 427.0483, 427.0001 $[M + H]^+$. IR (KBr pellets, cm^{-1}): 989, 1031, 1507, 1531, 1588. UV−vis (c, 1×10^{-5} M; CH_3CN; λ_{max} nm, ε M^{-1} cm^{-1}): 530 (2.37×10^4), 458 (7.97×10^4), 277 (7.09×10^4).

Synthesis of [Ni(4-pydpm)(dipdtc)] (2). It was prepared following the above procedure for **1** using $[Ni(dipdtc)_2]$. After workup and purification by column chromatography (SiO_2; CH_2Cl_2/hexane 50:50) complex **2** was isolated as red crystals. Yield: (0.091 g; 40%). Anal. Calcd for $C_{21}H_{24}N_4NiS_2$: C, 55.40; H, 5.31; N, 12.31. Found: C, 55.44; H, 5.29; N 12.37%. ^1H NMR ($CDCl_3$, δ_H ppm): 8.61, (d, 2H, J = 48 Hz, pyridyl), 7.31 (d, 2H, J = 51 Hz, pyridyl), 7.06 (s, 2H, pyrrole), 6.51 (d, 2H, J = 36 Hz, pyrrole), 6.41 (d, 2H, J = 36 Hz, pyrrole), 1.53 (m, 12H, $CH(C\underline{H}_3)_2$), 1.28 (m, 2H, $C\underline{H}(CH_3)_2$). ^{13}C NMR ($CDCl_3$, δ_C ppm): 201.22, 150.14, 149.56, 137.53, 135.46, 133.73, 131.57, 122.27, 117.98, 51.43, 19.67. ESI-MS. Calcd, found: m/z 455.0796, 455.0952 $[M + H]^+$. IR (KBr pellets, cm^{-1}): 995, 1033, 1510, 1534, 1595. UV−vis (c, 1×10^{-5} M; CH_3CN, λ_{max} nm, ε M^{-1} cm^{-1}): 530 (2.61×10^4), 457 (8.54×10^4), 278 (7.21×10^4).

Synthesis of Silver Nanoparticles (AgNPs) Using 1 and 2. Syntheses of AgNPs were achieved using CH_3CN solution of $AgNO_3$ (c, 1×10^{-2} M, 30 μL) and **1**/**2** (c, 1×10^{-4} M), employing different molar ratios of Ag/[**1**/**2**] (03, 1000 μL; 06, 500 μL; 10, 300 μL; 20, 150 μL), diluted to 10 mL using CH_3CN; the color of the solution turned lemon-yellow from brown-red. Aqueous cooled solution of $NaBH_4$ (c, 3×10^{-2} M, 80 μL) was added dropwise (10 min) to the resulting solution, whereupon color of the solution turned dark greenish-yellow from lemon-yellow. To avoid aggregation synthesized AgNPs were used without further purifications. The colloidal solution containing AgNPs is stable for more than a month as observed by UV−vis spectral studies.

X-ray Structure Determination. Single-crystal X-ray data for **1** was acquired on an R-AXIS RAPID II diffractometer using Mo Kα radiation (λ = 0.710 73 Å) at single-crystal X-ray diffraction center of the National Institute of Advanced Industrial Science and Technology (AIST), Osaka, Japan. The structure was solved by direct methods (SHELXS 97) and refined by full-matrix least-squares on F^2 (SHELX 97).[17] All the non-H atoms were treated anisotropically. H atoms attached to carbon were geometrically fixed and refined using SHELX riding model. The carbon atoms C35 and C36 are affected by thermal vibrational disorder and gave a prolate ellipsoid. To improve the bond length and thermal ellipsoid of N-ethyl group 27 least-squares restraints were used in the refinement. Further, structure was refined without fixing the occupational parameter of C35 and C36. Thus, the empirical formula does not match the calculated formula. Computer program PLATON was used for analyzing the interaction and stacking distances.[18] Additional crystallographic information is available in the Supporting Information.

Density Functional Theory Calculation. Theoretical studies on **1**, **1**·Ag^+ (NO_3^- excluded as a counteranion), and **1** with silver cluster Ag_n (n = 1, 3) were performed using GAUSSIAN 09/03 program

DOI: 10.1021/ic502848a
Inorg. Chem. 2015, 54, 2500−2511

package with the Becke three parameter exchange functional in conjunction with Lee−Yang−Parr correlation functional (B3LYP) method.[19,20] Geometries of the complexes were optimized using standard 6-31 G** basis set for C, H, N, and S and LANL2DZ for Ni and Ag.[21−23] Molecular electrostatic potential surfaces (MEPS) were also computed at the same level of density functional theory (DFT) calculation followed by geometry optimizations.

Catalytic Study. Reduction of 4-nitrophenol (4-NP) was performed in aqueous solution using standard quartz cell (path length, 1 cm; volume, 3.0 mL). In a typical experiment, 0.30 mL of the freshly prepared aqueous solution of $NaBH_4$ (15 mM) was introduced in the cuvette containing 4-NP (3.0 mL, 0.15 mM) at rt. It led to a distinct color change from light-yellow to yellow-green. It was further treated with samples containing silver nanoparticles (20 μL each, depending on the ratio) and followed by UV−vis spectroscopy at different time intervals in the scan range of 200−700 nm at rt.

RESULTS AND DISCUSSION

Synthesis and Characterization. The ligand 5-(4-pyridyl)dipyrromethane (4-pydpmH) was prepared by condensation of 4-pyridinecarboxaldehyde with an excess of pyrrole in the presence of catalytic amounts of trifluoroacetic acid (TFA) following literature procedures.[24] Heteroleptic dipyrrinato nickel(II) complexes [Ni(4-pydpm)(dedtc)] (**1**) and [Ni(4-pydpm)(dipdtc)] (**2**) were synthesized in poor to good yield (35−40%) by reacting in situ generated 4-pydpm [obtained by oxidation of 4-pydpmH (1 equiv) using DDQ] with $[Ni(dedtc)_2]/[Ni(dipdtc)_2]$ in the presence of triethylamine. Simple synthetic strategy adopted for the preparation of **1** and **2** is shown in Scheme 1.

Scheme 1. Synthesis of Complexes 1 and 2

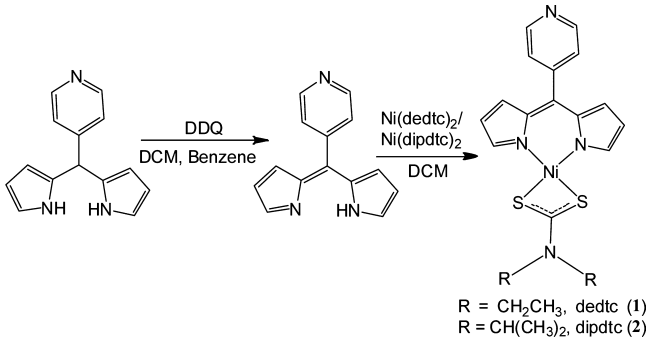

The complexes under investigation are crystalline, non-hygroscopic solids, soluble in common organic solvents such as methanol, ethanol, benzene, chloroform, dichloromethane, acetone, dimethyl sulfoxide, and dimethylformamide and insoluble in hexane, petroleum ether, and diethyl ether. These were thoroughly characterized by satisfactory elemental analyses, ESI-MS (Supporting Information, Figures S1 and S2), IR, ^{1}H, ^{13}C NMR, and UV−vis spectral studies. Molecular structure of **1** was determined by X-ray single-crystal analysis.

Infrared spectra strongly supported presence of both dtc and dipyrrin moieties in the complexes. The characteristic bands due to νC=N (S_2−C=NR_2) exhibited small shift of ∼6 cm^{-1} relative to the respective precursor complexes [1537, Ni(dedtc)$_2$; 1540 cm^{-1}, Ni(dipdtc)$_2$] and vibrated at ∼1531 (**1**) and 1534 cm^{-1} (**2**). The bidentate coordination of dtc moiety was evidenced by the presence of only one unsplitted intense band due to νC−S for **1** and **2** at ∼1031 and 1033 cm^{-1}, respectively.[25] In addition, vibrations associated with C=$N_{(pyrrol)}$ for coordinated 4-pydpm appeared as splitted band at 1507 (**1**) and 1510 cm^{-1} (**2**).[25,26]

The ^{1}H NMR spectra of **1** and **2** were acquired in deuterated chloroform ($CDCl_3$) at rt, and resulting data along with other characterization data is gathered in the Experimental Section; these spectra are depicted in the Supporting Information (Figures S3 and S4). The protons associated with 4-pydpm for both **1** and **2** exhibited deshielding and appeared at ∼7.03 (pyrrole), 6.47 (pyrrole), and 6.27 ppm (pyrrole), while pyridyl protons resonated at ∼8.68 and 7.36 ppm. The α and β protons related to the dedtc in **1** [N-(CH_2)$_2$(CH_3)$_2$; N-(CH_2)$_2$(CH_3)$_2$] displayed downfield shift of ∼0.02 ppm [∼3.66, 1.27 ppm]. Likewise, the protons for dipdtc in **2** resonated at almost their usual position [∼1.51, 1.27 ppm, **2**].[9,25,26] A small shift in the position of resonances due to both 4-pydpm and dtc protons may be ascribed to the formation of respective complexes. ^{13}C NMR spectra of **1** and **2** exhibited an analogous pattern of resonances and strongly supported proposed formulations. Most significant resonances associated with S_2−C=NR_2 carbon in these complexes resonated at 202.08 (**1**) and 201.22 ppm (**2**), which is consistent with earlier reports.[9,25,26] Overall NMR spectral data corroborated well with proposed formulation of the complexes.

Crystal Structure. Single crystals for X-ray diffraction studies were obtained by slow diffusion of hexane into a concentrated dichloromethane solution of **1** and **2**. We could not get quality crystals suitable for X-ray diffraction studies for **2**. Structure of **1** was determined crystallographically, detailed crystallographic data and selected geometrical parameters are summarized in Tables 1 and 2, and a pertinent view is given in Figure 1. It crystallizes in monoclinic system with $P2_1/c$ space group. Coordination geometry about the nickel(II) center in this complex may best be described as distorted square planar defined by S1/S2 from dedtc and N1/N2 from the 4-pydpm. Distortion from square planar geometry around the metal center may be attributed to small bite angles (N1−Ni−N2,

Table 1. Crystal Data and Structure Refinement Parameters for 1

empirical formula	$C_{19}H_{20}N_4Ni_1S_2$
crystal system	monoclinic
space group	$P2_1/c$
a (Å)	14.349(3)
b (Å)	15.726(3)
c (Å)	18.350(4)
α (deg)	90.00
β (deg)	108.45(3)
γ (deg)	90.00
V (Å^3), Z	3927.9(16), 4
λ (Å)	0.710 73
color and habit	red, block
T (K)	293(2)
reflns collected	34 949
refins/restraints/params	9002/27/474
D_{calcd} (mg m^{-3})	1.442
μ (mm^{-1})	1.210
GOF on F^2	1.103
final R indices $I > 2\sigma(I)$	$R1$ = 0.0524
	$wR2$ = 0.1541
R indices (all data)	$R1$ = 0.0717
	$wR2$ = 0.1648

DOI: 10.1021/ic502848a
Inorg. Chem. 2015, 54, 2500−2511

Table 2. Selected Bond Lengths (Å) and Angles (deg) for 1

bond length (Å)	1
Ni−N1	1.91(3)
Ni−N2	1.90(3)
Ni−S1	2.20(12)
Ni−S2	2.20(12)
C15−S1	1.71(5)
C15−S2	1.70(5)
C15−N4	1.33(5)
bond angle (deg)	
N2−Ni−N1	92.9(15)
N2−Ni−S1	94.5(11)
N1−Ni−S1	172.6(11)
N2−Ni−S2	172.4(11)
N1−Ni−S2	94.7(11)
S1−Ni−S2	77.9(5)
C15−S1−Ni1	86.5(16)
C15−S2−Ni1	86.9(16)
N4−C15−S1	125.3(4)
N4−C15−S2	126.1(4)
S2−C15−S1	108.6(2)
ω^a	69.09

[a] ω = the twist angle between dipyrrin core and *meso*-phenyl substituent.

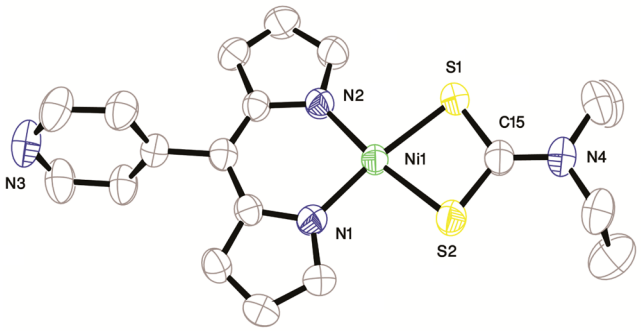

Figure 1. ORTEP view of **1** at 50% thermal ellipsoid probability (H atoms omitted for clarity).

92.9° and S1−Ni−S2, 77.9°). The Ni−N [Ni−N1, 1.91; Ni−N2, 1.90 Å] and Ni−S [Ni−S1, 2.20; Ni−S2, 2.20 Å] bond distances and various angles [N1−Ni−N2, 92.9; S1−Ni−S2, 77.9; N1−Ni−S1, 94.5; N2−Ni−S2, 94.7°] are normal and comparable to those in other related systems.[9,27,28] The C15−N4 bond distance is shorter (1.33 Å) relative to other C−N bond distances indicating occurrence of double-bond character. An increase in the S−C−N bond angle (S1−C15−N4, 125.3; S2−C15−N4, 126.1°) arises from delocalization of the π-electron density over S2CN moiety. The S1−C15−S2 bite angle is 108.6°, and *meso*-pyridyl substituent is twisted out of the plane with respect to dipyrrin unit by 69.09°. All these parameters are in good agreement with the earlier reports.[9,10,27,28]

Weak bonding interaction studies on this complex revealed presence of various types of interactions leading to interesting motifs. Complex **1** exhibited a polymeric chain arising from C−H···N (3.445 Å) interactions (Figure 2). It also displayed helical structure resulting from C−H···π interactions with alternate bond lengths of 3.560 and 3.579 Å (Supporting Information, Figure S7).[29]

UV−vis Spectroscopy. Electronic absorption spectra of **1** and **2** were acquired in acetonitrile (c, 10 μM), and resulting data along with other information is congregated in the Experimental Section. Interesting feature of the UV−vis spectra of these complexes is presence of intense low- and high-energy absorptions at ∼458 nm [458, **1**; 457 nm **2**] and ∼277 nm [277, **1**; 278 nm **2**]. On the basis of its intensity and position these were tentatively assigned to the $\pi-\pi^*$ charge-transfer transitions associated with conjugated dipyrrinato moiety and intraligand $\pi-\pi^*$ transitions (Figure 3).[9,10,27] In addition, both the complexes exhibited a broad hump at ∼530 nm, which was tentatively assigned to the metal-to-ligand charge-transfer (MLCT) transition.

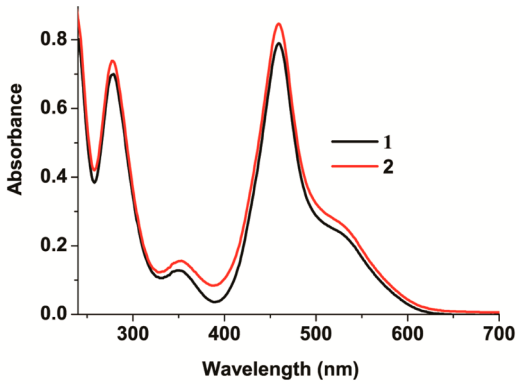

Figure 3. UV−vis absorption spectra of **1** and **2** (c, 1 × 10^{-5} M; CH_3CN).

Electrochemical Studies. Redox behavior of **1** and **2** were followed by cyclic (CV) and differential pulse voltammetry (DPV) in the potential range from +2.0 to −2.0 V in CH_3CN (c, 100 μM) at rt and scan rate of 100 mV s^{-1} using 0.1 M [(*n*-Bu)$_4$N]ClO_4 as a supporting electrolyte. Resulting voltammograms for **1** and **2** are depicted in Figure 4. In their CV both **1** and **2** exhibited two quasi-reversible oxidation waves at (E_{pa} = 0.564 V, **1**; 0.569 V **2**) and (E_{pa} = 0.866 V **1**; 0.871 V **2**) assignable to dpm/dpm$^+$ and Ni^{2+}/Ni^{3+} redox couple.[9,10,27] Accordingly, these displayed a distinctive peak in their DPV (E_{pa} = 0.522 V, **1**; 0.524 V **2**; E_{pa} = 0.805 V, **1**; 0.818 V, **2**) due to aforesaid (dpm/dpm$^+$ and Ni^{2+}/Ni^{3+}) redox couples.

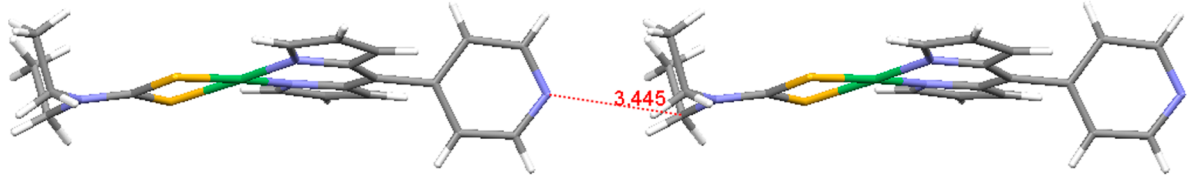

Figure 2. Extended one-dimensional chain arising from C−H···N interactions along crystallographic "*a*" axis.

DOI: 10.1021/ic502848a
Inorg. Chem. 2015, 54, 2500−2511

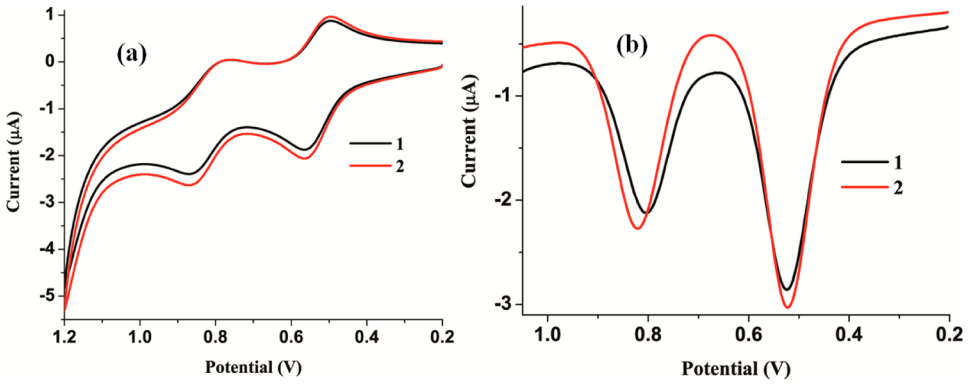

Figure 4. Cyclic (a) and differential pulse voltammograms (b) for **1** and **2** (c, 100 μM; CH_3CN).

Characterization of Silver Nanoparticles by UV–vis Spectral Studies. UV–vis absorption spectroscopy is one of the simplest, highly sensitive, and most extensively used techniques for the characterization of nanoparticles. Formation of the AgNPs was followed by absorption spectral studies on synthesized nanoparticles (range of 200–800 nm). It is well-known that the position and shape of surface plasmon absorption band strongly depends on the particle size, shape, and dielectric constant of the medium.[7,30] Molar ratio of the reducing agent ($NaBH_4$) required for formation of nanoparticles was optimized by UV–vis spectral studies. It was observed that 80 μL of $NaBH_4$ (c, 3×10^{-2} M) is sufficient for complete reduction of silver(I)-nitrate ($AgNO_3$) (c, 1×10^{-2} M, 30 μL). Concentration and amount of both $AgNO_3$ (c, 1×10^{-2} M, 30 μL) and $NaBH_4$ (c, 3×10^{-2} M, 80 μL) were fixed throughout the experiment; only the amounts of **1** and **2** were varied. As well, one can have an idea about the formation and optical properties of AgNPs from color changes and UV–vis spectra of the resulting solution (Figures 5–7).

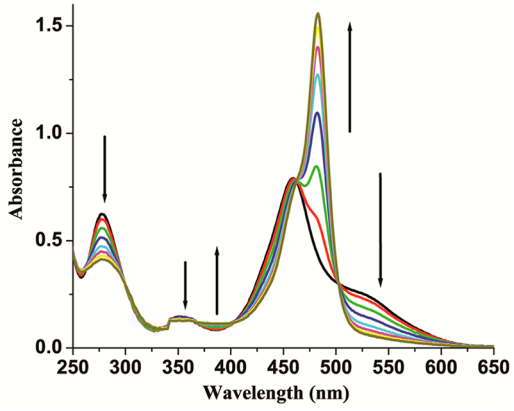

Figure 5. UV–vis absorption spectra of **1** (c, 1×10^{-5} M; CH_3CN) upon addition of increasing concentrations of Ag^+ (0.0–5.0 equiv).

To verify the possibility of formation of NiNPs from **1**/**2**(c, 1×10^{-4} M, 4 mL) different concentrations and amounts of $NaBH_4$ (c, 3×10^{-2} M, 500 μL; c, 3×10^{-1} M, 100 μL; c, 3×10^{-1} M, 500 μL and c, 3 M, 100 μL) were directly added to a solution of the said complexes, and total volume was maintained at 6 mL by addition of CH_3CN. Observed color changes at different time intervals (0, 6, 12, 18, 24 h) are shown in Figure S8 (Supporting Information). Addition of $NaBH_4$ (c, 3×10^{-2} M, 500 μL) to a solution of complexes did not show any appreciable color change even after 24 h. On the other hand, slightly higher concentration of $NaBH_4$ (c, 3×10^{-1} M, 100 μL) led to a small color change and distinct color changes (from brown-red to colorless) at higher concentrations (c, 3×10^{-1} M, 500 μL and c, 3 M, 100 μL). From this study it is concluded that addition of up to 500 μL of $NaBH_4$ does not show formation of NiNPs. Further, to investigate formation of the silver nanoparticles, $AgNO_3$ (5 μL; c, 1×10^{-2} M) was added to a solution of **1**/**2**. It was observed that hump at ~530 nm in the UV–vis spectrum of **1**/**2** diminished, whereas the band at ~458 nm exhibited a small decrease in the absorption intensity with red shift of 4 nm. Simultaneously, a new band emerged at ~482 nm, and color of the solution became lemon-yellow (Figures 5–7).

To understand the binding affinity and sensitivity of **1** toward Ag^+ ions, absorption titration studies were carried out. Gradual addition of Ag^+ (0–5.0 equiv) to a solution of **1**(c, 1×10^{-5} M) causes loss of the band at 530 nm and hypochromism for the band at 458 nm with red shift of 4 nm (462 nm). A new band emerged at ~482 nm, while the one at 277 nm (Figure 5) also displayed hypochromism. Appearance of distinct isosbestic points at 502, 462, 402, 341, 299, and 261 nm in the titration curve is consistent with equilibrium between **1** and **1**·Ag^+ in solution (Figure 5). Association constant for **1** (4.12×10^3 $M^{-1/2}$) toward Ag^+ was determined by Benesi–Hildebrand method, and Job's plot analysis indicated a 2:1 stoichiometry between **1** and Ag^+ (Supporting Information, Figure S9). Reversibility of system was affirmed by adding Ag^+ (5.0 equiv) and an excess of ethylenediaminetetraacetic acid (25.0 equiv)

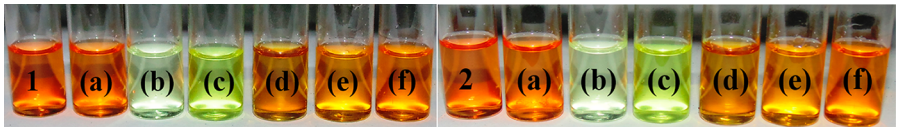

Figure 6. Color changes for **1**/**2** with $NaBH_4$ (c, 3×10^{-2} M, 500 μL, after 24 h) (a), color changes for **1**/**2** with $AgNO_3$ (c, 1×10^{-2} M, 5 μL) (b) and silver nanoparticles varying ratio of Ag/[**1**/**2**] = 03 (c), 06 (d), 10 (e), and 20 (f).

DOI: 10.1021/ic502848a
Inorg. Chem. 2015, 54, 2500–2511

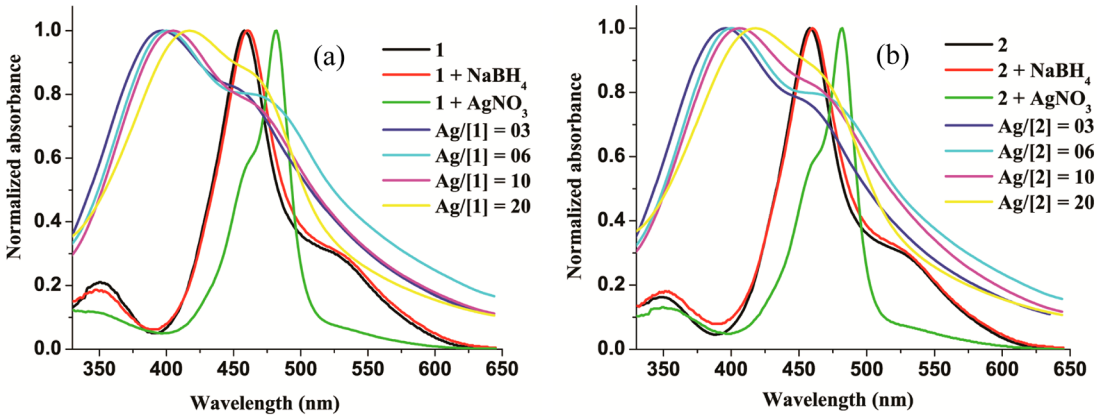

Figure 7. Absorption spectra of **1** (a), **2** (b), and AgNPs with respect to varying Ag/[**1**/**2**] (ratios 03, 06, 10, and 20). The spectra are normalized at maximum value of surface plasmon band, observed at ∼400 nm.

Scheme 2. Plausible Mechanism for the Formation of AgNPs and Schematic View of the Proposed Orientation of 1/2 at the Surface of AgNPs

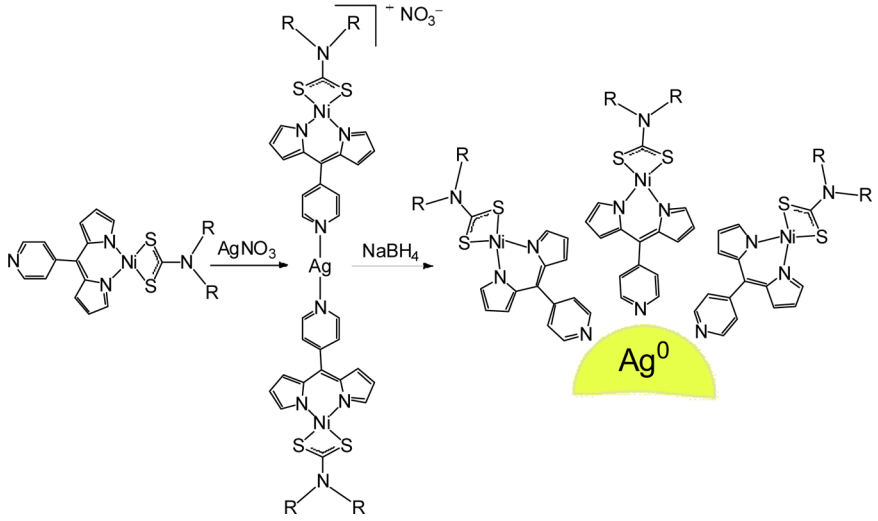

(Supporting Information, Figure S10). It resulted in restitution of the absorption band at ∼531 and 457 nm indicating regeneration of **1** and reversible binding.

To gain better understanding of the complexation behavior of **1** with Ag^+, ^1H NMR titration studies were performed in $(CD_3)_2SO$, and resulting spectral differences are depicted in Figure S11 (Supporting Information). Complexation of **1** with Ag^+ is expected to reduce electron density about the coordination site and induce a downfield shift for nearby protons. As expected, in the presence of Ag^+ pyridyl protons 6 and 7 exhibited distinct downfield shifts ($\Delta\ \delta$, 0.251, 6; 0.534 ppm 7) along with broadening of the signals. On the other hand, protons due to pyrrolic and dedtc moiety resonated at their usual position (except 3 and 4, which merged into a single peak) with broadening. Obvious changes in the chemical shifts indicated that **1** could form a stable complex with Ag^+ through pyridyl nitrogen as shown in Scheme 2. From the above study it is concluded that nanoparticle formation does not occur after addition of $AgNO_3$ to a solution of **1**/**2** (characterized by TEM studies). Simultaneously, dropwise addition of $NaBH_4$ to a mixture of $AgNO_3$ and **1**/**2** led to intense greenish-yellow color and displayed surface plasmon band at ∼400 nm, affirming formation of the AgNPs. Details about synthesis and UV−vis spectral studies are given in Experimental Section and vide infra.

Usually, unprotected AgNPs exhibit an absorption band with a maximum at ca. 390 nm. UV−vis spectra of the synthesized AgNPs with varying Ag/[**1**/**2**] ratio (03, 06, 10, 20) are shown in Figure 7. Clearly, both **1**/**2** exhibit characteristic surface plasmon (SP) resonances for spherical AgNPs [created by addition of Ag/[**1**/**2**] (ratio; 03; average particle size ≈ 10 ± 2 nm)] at ∼395 nm, which was also followed by TEM measurements. Shift in the position of SP band (390 nm, unprotected AgNPs) by capping silver particles may be attributed to bond formation between Ag clusters and free pyridyl nitrogen from **1**/**2**. The UV−vis spectrum also exhibited typical bands due to $\pi-\pi^*$ transitions corresponding to conjugated dipyrrinato ligands, which strongly supported presence of the dipyrrin core.

The EDX-STEM analyses on particles revealed presence of **1**/**2** around silver colloids (Figure 8). Further, additions of Ag/[**1**/**2**] (ratios 06 and 10) displayed a small red shift of ∼3 and 10 nm for the SP band (398 nm, 06; 405 nm, 10) and an increase in the particle size to ∼15 and 20 nm, respectively (characterized by TEM analysis). Moreover, an excess of Ag/[**1**/**2**] (ratio 20) resulted in a significant red shift of ∼22 nm

DOI: 10.1021/ic502848a
Inorg. Chem. 2015, 54, 2500−2511

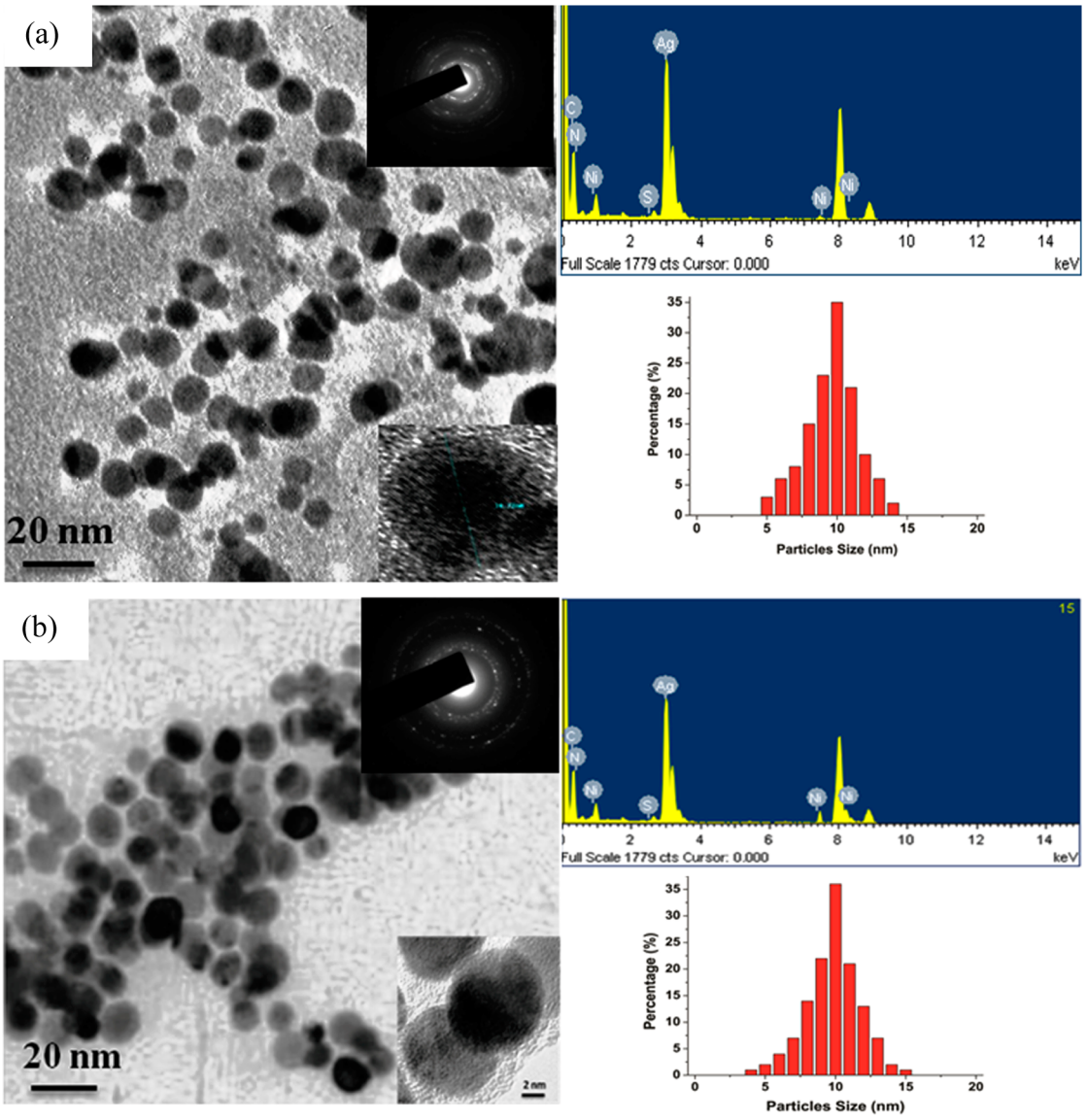

Figure 8. TEM images, electron diffraction pattern (inset), EDX analysis (inset), and size distribution histogram of silver-coated nanoparticles, ratio of Ag/[**1**] (03) (a) and Ag/[**2**] (03) (b).

(417 nm) and aggregation of the particles, which is supported by TEM studies (vide infra).

A simple experiment was also carried out to investigate the probability for the formation of NiNPs from AgNPs in the presence of $NaBH_4$. In this direction **1**/**2** were added to a solution containing AgNPs along with $NaBH_4$ (c, 3×10^{-2} M, 100 μL). Insignificant changes were observed for the SP band except more prominent band for dipyrrin core (Supporting Information, Figure S12). From this result, we exclude the possibilty of formation of NiNPs from AgNPs in the presence of $NaBH_4$.

From UV−vis absorption studies it is clear that wavelength of the SP band depends on particle size. It is evidenced by an increase in the wavelength (λ_{max}) of SP band from 395 to 417 nm for nanoparticles of different size. Colloidal solutions of the complexes are stable for over one month as evidenced by UV−vis spectroscopy. Red shift is also accompanied by slight broadening of the SP band toward long wavelength region. From UV−vis spectral studies we conclude that size of the nanopartilces can be controlled by varying the ratio of capping agents. Also, it was shown that it involves strong interaction between **1**/**2** and surface of the nanoparticles. Further, Ag/[**1**/**2**] ratio indicated that only a small amount of **1**/**2** is sufficient for effective coating of the AgNPs surface and provide stability in solution.

Transmission Electron Microscopy. Nanoparticle core dimensions are usually determined by TEM and HRTEM studies. TEM studies were performed to validate the formation of NiNPs from **1**/**2** by adding $NaBH_4$ (c, 3×10^{-2} M, 80 μL), and these studies revealed irregular rod- and flower-like aggregates (Supporting Information, Figure S13). Similarly, TEM images of the solution obtained by addition of $AgNO_3$ to a solution of **1**/**2** exhibited an analogous morphology (Supporting Information, Figure S14). From this study it is concluded that either NiNPs or AgNPs are not formed under these conditions.

TEM images of AgNPs resulting from addition of Ag/[**1**/**2**] (ratio 03) along with their electron-diffraction pattern, EDX spectroscopy, and corresponding particle size are depicted in Figure 8. From the TEM micrographs it is clear that AgNPs are

DOI: 10.1021/ic502848a
Inorg. Chem. 2015, 54, 2500−2511

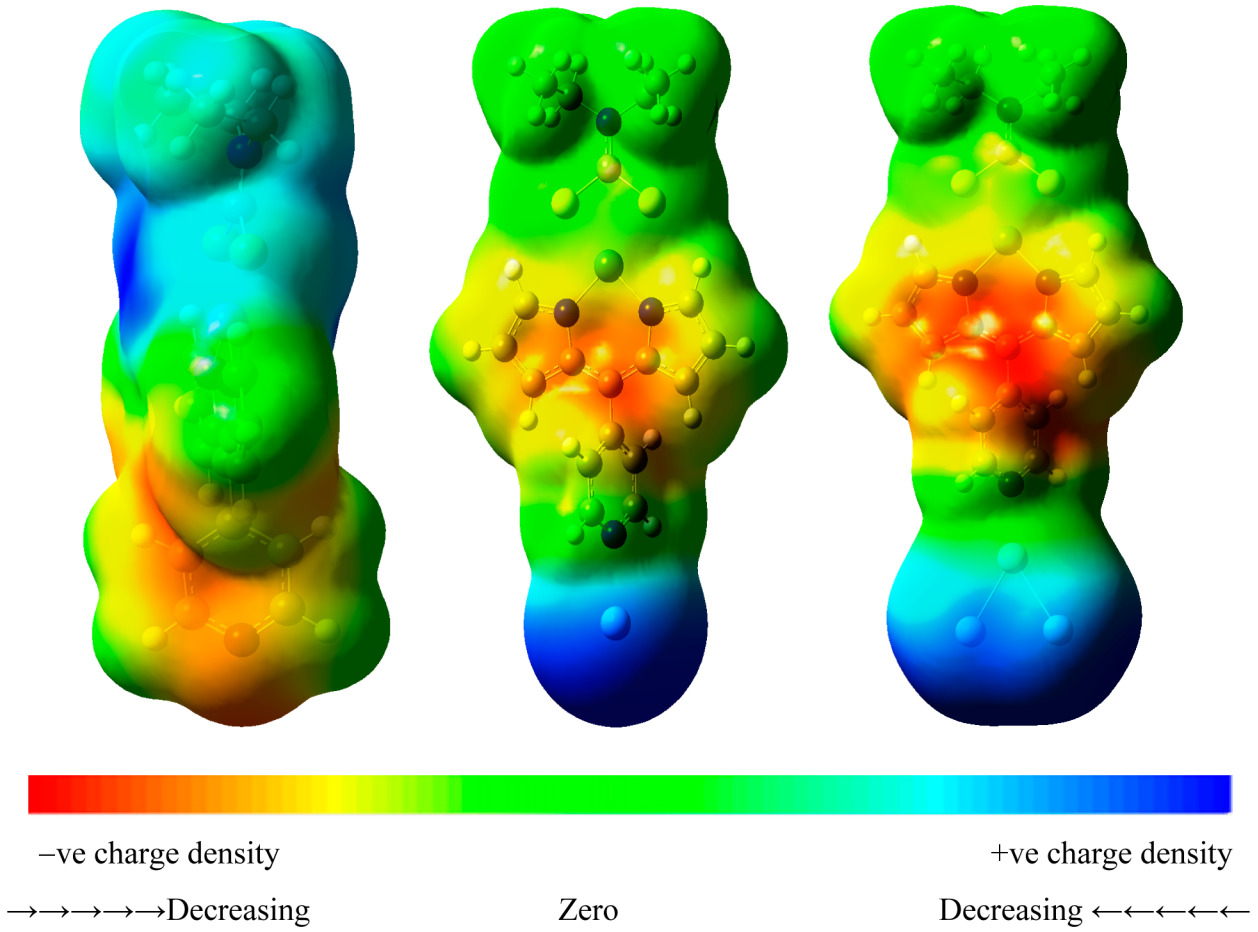

Figure 9. Molecular electrostatic potential surfaces of optimized structure **1** and its silver cluster Ag_n (n = 1, 3). In MEPS, color scheme: red/yellow—nucleophilic reaction site (highest −ve charge density) and blue/light blue—electrophilic site (highest +ve charge density).

well-dispersed spherical particles with average size of 10 ± 2 nm. The EDX analyses on AgNPs affirmed presence of a dipyrrin moiety along with silver and nickel (Figure 8) and suggested strong binding of the pyridyl nitrogen from dipyrrin moiety onto the Ag surface. This observation is consistent with earlier reports by Mayer et al.[13d,f,g] Further, it was observed that addition of Ag/[**1**/**2**] (ratio 06 and 10) led to an increase in the average size of AgNPs (Ag/[**1**/**2**] (06, 15 ± 2; 10, 20 ± 2 nm) without any significant aggregation (Supporting Information, Figures S15−S18). However, an increase in the ratio of Ag/[**1**/**2**] (20) resulted in aggregation of the particles (Supporting Information, Figure S19). Our observations further supported Mie theory and explained red shift of the SP resonances.[31] From the TEM studies it is concluded that size of the nanoparticles strongly depend on the ratio of Ag/[**1**/**2**] and is consistent with the conclusions drawn from UV−vis spectral studies.

To confirm the role of pyridyl nitrogen and sulfur from dtc moiety, we synthesized two more complexes Ni(4-pydpm)(acac) (**3**) (acac = acetylacetone) and Ni(phdpm)(dedtc) (**4**) (phdpm = 5-phenyldipyrromethene). From the UV−vis spectra and TEM images (Supporting Information, Figures S20 and S22) it is clear that **3** also leads to the stabilization of the AgNPs [Ag/[**3**], (ratio 03) similar to **1**. However, **4** exhibited destabilization and agglomeration of the bare AgNPs (Supporting Information; details about the preparation of **3**, **4**, and their AgNPs are given Figure S21). From this study we conclude that pyridyl group is crucial for stabilization of the AgNPs, while dtc plays insignificant role in this regard. TEM images of PVP-stabilized AgNPs [Ag/[PVP], ratio; 03] exhibited spherical particles with average size of 15 ± 4 nm (details of preparation are given in Supporting Information, Figures S23 and S24).

Overall results from the UV−vis and TEM studies clearly established that **1**/**2** behave as a good capping agent and free nitrogen from pyridyl group present as *meso* substituent in dipyrrin core is responsible for this activity. It is also observed that size of the AgNPs strongly depends on the ratio of Ag/[**1**/**2**] employed in the reaction. A simple schematic presentation displaying synthesis of AgNPs and arrangement of **1**/**2** about the silver in AgNPs is depicted in Scheme 2.

Density Functional Theoretical Studies. To understand the interaction of **1** with Ag^+, structures of **1** and **1**·Ag^+ (NO_3^- as a counteranion excluded) were optimized by DFT calculations. From the optimized structure, the difference between the total energy of **1** (−1920 au) and **1**·Ag^+ (−3987 au) is −2067 au, which signifies stability of **1**·Ag^+. Further, the MEPS of **1** revealed that maximum electron density (red) is localized on the pyridyl nitrogen, which forms a stable species by binding with Ag^+ (Figure 9 and Supporting Information, Figures S25a,b and S26).

Geometry optimizations on **1** and **1** with silver cluster (Ag_n; n = 1, 3) was performed to confirm the interaction/coordination site of **1** with AgNPs. The most plausible and completely converged optimized geometry of **1** with silver cluster near nitrogen of the pyridyl group is shown in Figure

DOI: 10.1021/ic502848a
Inorg. Chem. 2015, 54, 2500−2511

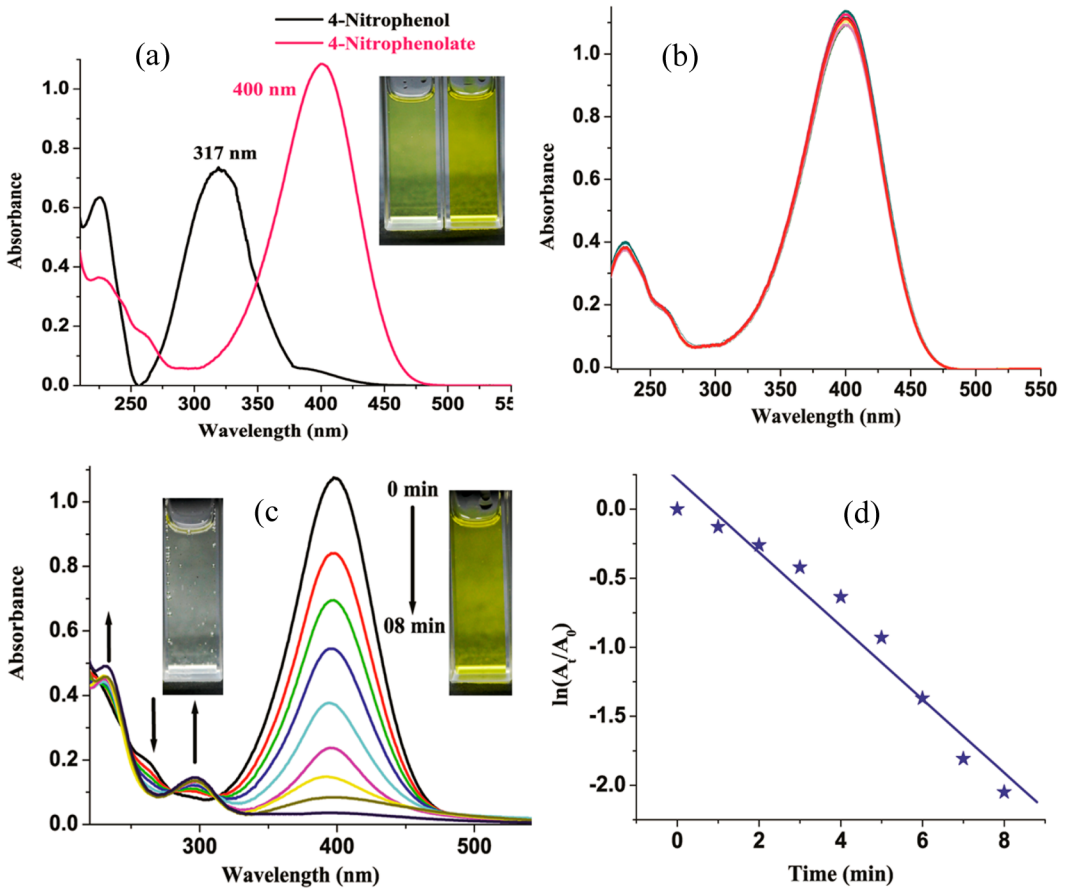

Figure 10. UV−vis spectra of 0.15 mM 4-NP before and after addition of 15 mM $NaBH_4$ solution (a); 0.15 mM 4-NP with 15 mM $NaBH_4$ without any catalyst (b); 0.15 mM 4-NP with 15 mM $NaBH_4$ in the presence of AgNPs (Ag/[**1**] ratio 03) as catalyst at rt (c); and plot of $\ln(A_t/A_0)$ vs. reaction time showing pseudo- first order kinetics.

Table 3. Summary of the Molar Ratios and Apparent Rate Constant for Different Experiments[a]

complex	ratio Ag/[**1**/**2**]	$AgNO_3$	average diameter	absorbance λ_{max} (nm)	k_{app} (min^{-1})	time (min) for 4-NP to 4-AP conversion
1	03	1×10^{-2} M (30 μL)	10 ± 2 nm	395	0.371	08
	06	1×10^{-2} M (30 μL)	15 ± 2 nm	398	0.319	10
	10	1×10^{-2} M (30 μL)	20 ± 2 nm	405	0.281	15
	20	1×10^{-2} M (30 μL)	aggregation	417	0.215	20
2	03	1×10^{-2} M (30 μL)	10 ± 2 nm	395	0.368	08
	06	1×10^{-2} M (30 μL)	15 ± 2 nm	398	0.312	10
	10	1×10^{-2} M (30 μL)	20 ± 2 nm	405	0.279	15
	20	1×10^{-2} M (30 μL)	aggregation	417	0.201	20
PVP		1×10^{-2} M (30 μL)	15 ± 4 nm	400	0.123	45

[a]The volume (80 μL) of cooled aqueous $NaBH_4$ (c, 3×10^{-2} M) solution was fixed throughout the experiment for AgNPs preparation. For catalytic reduction of 4-NP to 4-AP, 20 μL of AgNPs with ratio Ag/[**1**/**2**] = 03, 06, 10, and 20 were used.

S25c,d (Supporting Information). Geometry optimization of **1** with Ag_1 near the sulfur of dtc moiety was also tried (five times) to understand the possible interaction site, but it shows convergence failure using same method. MEPS are very useful descriptors to determine the electron density, sites for electrophilic and nucleophilic reaction, as well as structure−reactivity relationship of the molecules. Therefore, MEPS were computed to deduce the coordination sites more precisely for Ag_n with **1**. The MEPS of optimized **1** and its Ag_n (n = 1, 3) cluster are illustrated in Figure 9. We observed that electron density (red) is localized mostly on pyridyl nitrogen; therefore, Ag^0 coordinates to it. After coordination of Ag^0 to pyridyl nitrogen the electron density is shifted toward dipyrrin moiety (Figure 9).

Catalytic Reduction. Reduction of 4-nitrophenol (4-NP) to 4-aminophenol (4-AP) in the presence of $NaBH_4$ in an aqueous medium at rt is generally taken as a model reaction to establish the catalytic efficacy of metal nanoparticles.[32] Such a reaction is of utmost interest in the synthesis of widely used pharmaceuticals, for example, paracetamol.[5] Catalytic activity of the prepared AgNPs was evaluated toward aforesaid reduction. It is well-known that 4-NP exhibits light yellow color and displays an absorption band at ∼317 nm.[32,33] Addition of a reducing agent like $NaBH_4$ to its solution leads to a distinct color change from light to intense yellow due to formation of 4-

DOI: 10.1021/ic502848a
Inorg. Chem. 2015, 54, 2500−2511

nitrophenolate ion.[32,33] Color change results from alteration in the pH (acidic to highly basic) of solution in the presence of $NaBH_4$, leading to a marked shift in the position of absorption band (Figure 10a).

Progress of the catalytic reaction can be followed by monitoring changes in the position of characteristic band due to 4-nitrophenolate ion by UV−vis spectroscopy. Notably, absorption band due to 4-nitrophenolate ion centered at 400 nm does not show any significant change in its intensity and position, only in the presence of $NaBH_4$ even after 2 h (Figure 10b), which clearly rules out possibility of the reduction in absence of a catalyst. However, addition of a trace amount of the prepared AgNPs (20 μL of AgNPs with Ag/[**1**/**2**] (ratio 03, 06, 10, and 20) led to emergence of a new band at ∼295 nm with gradual increase in its intensity, indicating reduction of the 4-NP and formation of 4-AP (Table 3). In addition, UV−vis spectra also exhibited two isosbestic points at ∼280 and ∼312 nm suggesting reduction of 4-NP exclusively to 4-AP without any other side products (Figure 10 and Supporting Information, Figures S27−S33).[33]

To compare the catalytic efficiency of the synthesized AgNPs an experiment was also performed using PVP-stabilized AgNPs. It requires relatively higher amount (100 μL) and takes more time (45 min) relative to the synthesized AgNPs employing metal complexes (**1**/**2**) (Supporting Information, Figure S34). It may be attributed to the synergistic effect of metal (Ni) present in the synthesized complex. Further, to examine the role of capping agent **1**/**2** (c, 1×10^{-4} M; 75 μL) itself in the catalytic reaction, a control experiment using **1**/**2** was carried out with 4-nitrophenolate under analogous conditions. Notably, it showed insignificant changes in the presence of the capping agent **1**/**2**, only (Supporting Information, Figure S35). This finding clearly revealed that for catalytic reduction, the presence of the AgNPs is a must.

It is presumed that catalytic cycle follows pseudo-first-order kinetics with respect to 4-NP. Consequently, ratio of the absorbance (A_t) of 4-NP at time t to the absorbance (A_0) at t = 0 must be equal to the concentration ratio (C_t/C_0) for 4-NP. Thus, the kinetic equation for catalytic reduction can be given as

$$\ln(C_t/C_0) = \ln(A_t/A_0) = -k_{app}t$$

where C_t is the concentration of 4-NP at time t, and k_{app} is the apparent rate constant. From the plot of $\ln(A_t/A_0)$ versus time a good linear correlation was obtained, which validated that reaction indeed follows pseudo-first-order kinetics and that apparent rate constant k_{app} can be calculated using the above equation. Value of the resulting rate constants given in Table 3 are consistent with earlier reports.[34] From the values it is clear that AgNPs arising from Ag/[**1**/**2**] = 03 molar ratio exhibit highest catalytic efficiency relative to other ratios and may be attributed to large surface area of the nanoparticles (Table 3).

CONCLUSIONS

In summary, through this work we have presented syntheses and characterizations of two new heteroleptic dipyrrinato complexes appended with dialkyldithiocarbamate and dipyrrin ligands having 4-pyridyl group as a *meso* substituent. The complexes under study have been successfully utilized as capping agent in the synthesis of AgNPs through nonconventional nitrogen from pyridyl group. Core diameter of the synthesized nanoparticles lie within 10−20 nm and strongly depend on the ratio of Ag/[**1**/**2**] = 03, ∼10 nm; 06, ∼15 nm; 10, ∼20 nm as attested by TEM measurements. Synthesized AgNPs have been successfully employed as efficient catalysts for reduction of 4-nitrophenol. It is noteworthy to mention that pyridyl group plays an important role in stabilization of the AgNPs, whereas dithiocarbamate moiety shows insignificant role. We believe that the present protocol may pave the way for synthesis of nanoparticles based on the metal complexes, which may find application in diverse areas.

ASSOCIATED CONTENT

Supporting Information

^1H and ^{13}C NMR spectra, ESI-MS data, TEM images, optimized structures, UV−vis spectra, and plots of 4-NP reduction are given. This material is available free of charge via the Internet at http://pubs.acs.org. CCDC No. 992296 (**1**) contains the supplementary crystallographic data for this paper. It can be had free of charge via https://summary.ccdc.cam.ac.uk/structure-summary-form (or from the CCDC, 12 Union Road, Cambridge CB2 1EZ, U.K.; Fax: +44−1223−336033; E-mail: deposit@ccdc.cam.ac.uk).

AUTHOR INFORMATION

Corresponding Author

*E-mail: dspbhu@bhu.ac.in.

Notes

The authors declare no competing financial interest.

ACKNOWLEDGMENTS

Authors thank the Department of Science and Technology, New Delhi, India, for financial assistance through the Scheme (SR/S1/IC/-25/2011) and the Council of Scientific and Industrial Research (CSIR) New Delhi, India, for the award of a Junior Research Fellowship to R.K.G. (No. 09/013(0210)/2009-EMR-I). We are also thankful to the Head, Dept. of Chemistry, Faculty of Science, Banaras Hindu Univ., Varanasi (U.P.) India, for extending laboratory facilities and to the National Institute of Advanced Industrial Science and Technology (AIST), Osaka, Japan, for providing single-crystal X-ray data.

REFERENCES

(1) (a) Ghosh, S. K.; Pal, T. *Chem. Rev.* **2007**, *107*, 4797−4862. (b) Mirkin, C. A.; Letsinger, R. L.; Mucic, R. C.; Storhoff, J. J. *Nature* **1996**, *382*, 607−609. (c) Crooks, R. M.; Zhao, M.; Sun, L.; Chechik, V.; Yeung, L. K. *Acc. Chem. Res.* **2001**, *34*, 181−190. (d) Kelly, K.; Coronado, L. E.; Zhao, L. L.; Schatz, G. C. *J. Phys. Chem. B* **2003**, *107*, 668−677. (e) Gittins, D. I.; Bethell, D.; Schiffrin, D. J.; Nichols, R. J. *Nature* **2000**, *408*, 67−69. (f) Kyriacou, S. V.; Brownlow, W. J.; Xu, X.-H. N. *Biochemistry* **2004**, *43*, 140−147. (g) Rao, C. N. R.; Kulkarni, G. U.; Thomas, P. J.; Edwards, P. P. *Chem.—Eur. J.* **2002**, *8*, 28−35. (h) Qin, B.; Chen, H.; Liang, H.; Fu, L.; Liu, X.; Qiu, X.; Liu, S.; Song, R.; Tang, Z. *J. Am. Chem. Soc.* **2010**, *132*, 2886−2888. (i) Gong, J.; Zhou, F.; Li, Z.; Tang, Z. *Langmuir* **2012**, *28*, 8959−8964. (j) Gong, J.; Zhou, F.; Li, Z.; Tang, Z. *Chem. Commun.* **2013**, *49*, 4379−4381.

(2) (a) Agnihotri, S.; Mukherji, S.; Mukherji, S. *RSC Adv.* **2014**, *4*, 3974−3983. (b) Sun, Y.; Xia, Y. *Science* **2002**, *298*, 2176−2179. (c) Bois, L.; Chassagneux, F.; Desroches, C.; Battie, Y.; Destouches, N.; Gilon, N.; Parola, S.; Stéphan, O. *Langmuir* **2010**, *26*, 8729−8736. (d) Dong, X.; Ji, X.; Wu, H.; Zhao, L.; Li, J.; Yang, W. *J. Phys. Chem. C* **2009**, *113*, 6573−6576.

(3) (a) Noguez, C. *J. Phys. Chem. C* **2007**, *111*, 3806−3819. (b) Noguez, C. *Opt. Mater.* **2005**, *27*, 1204−1211. (c) Tao, A.; Sinsermsuksakul, P.; Yang, P. *Angew. Chem., Int. Ed.* **2006**, *45*, 4597−

DOI: 10.1021/ic502848a
Inorg. Chem. 2015, 54, 2500−2511

4601. (d) Barnard, A. S.; Lin, X. M.; Curtiss, L. A. *J. Phys. Chem. B* **2005**, *109*, 24465−24472. (e) Gebauer, D.; Cölfen, H. *Nano Today* **2011**, *6*, 564−584.
(4) (a) Lok, C. N.; Ho, C. M.; Chen, R.; He, Q.; Yu, Y. W. Y.; Sun, H.; Tam, P. K. H.; Chiu, J. F.; Che, C. M. *J. Proteome Res.* **2006**, *5*, 916−924. (b) Gunawan, P.; Guan, C.; Song, X.; Zhang, Q.; Leong, S. S. J.; Tang, C.; Chen, Y.; Chanpark, M. B.; Chang, M. W.; Wang, K.; Xu, R. *ACS Nano* **2011**, *5*, 10033−10040. (c) Morones, J. R.; Elechiguerra, J. L.; Camacho, A.; Holt, K.; Kouri, J. B.; Ramírez, J. T.; Yacaman, M. J. *Nanotechnology* **2005**, *16*, 2346−2353. (d) Dunn, K.; Edwards-Jones, V. *Burns* **2004**, *30*, S1−S9.
(5) (a) Liu, J.; Qin, G.; Raveendran, P.; Ikushima, Y. *Chem.—Eur. J.* **2006**, *12*, 2131−2138. (b) Murugadoss, A.; Chattopadhyay, A. *J. Phys. Chem. C* **2008**, *112*, 11265−11271. (c) Marcelo, G.; Munoz-Bonilla, A.; Fernandez-Garcia, M. *J. Phys. Chem. C* **2012**, *116*, 24717−24725.
(6) (a) Saha, S.; Pal, A.; Kundu, S.; Basu, S.; Pal, T. *Langmuir* **2010**, *26*, 2885−2893. (b) Rana, S.; Parida, K. M. *Catal. Sci. Technol.* **2012**, *2*, 979−986.
(7) (a) Rode, C. V.; Vaidya, M. J.; Jaganathan, R.; Chaudhari, R. V. *Chem. Eng. Sci.* **2001**, *56*, 1299−1303. (b) Vaidya, M. J.; Kulkarni, S. M.; Chaudhari, R. V. *Org. Process Res. Dev.* **2003**, *7*, 202−208.
(8) (a) Noguez, C. *Opt. Mater.* **2005**, *27*, 1204−1211. (b) Tao, A.; Sinsermsuksakul, P.; Yang, P. *Angew. Chem., Int. Ed.* **2006**, *45*, 4597−4601. (c) Chen, S.; Carroll, D. L. *Nano Lett.* **2002**, *2*, 1003−1007. (e) Maillard, M.; Giorgio, S.; Pileni, M.-P. *Adv. Mater.* **2002**, *14*, 1084−1086.
(9) (a) Ziessel, R.; Harriman, A. *Chem. Commun.* **2011**, *47*, 611−631. (b) Smalley, S. J.; Waterland, M. R.; Telfer, S. G. *Inorg. Chem.* **2009**, *48*, 13−15. (c) Ulrich, G.; Ziessel, R.; Harriman, A. *Angew. Chem., Int. Ed.* **2008**, *47*, 1184−1201. (d) Loudet, A.; Burgess, K. *Chem. Rev.* **2007**, *107*, 4891. (e) Swamy, P.; Chinna, A.; Thilagar, P. *Inorg. Chem.* **2014**, *53*, 2776−2786. (f) Wood, T. E.; Thompson, A. *Chem. Rev.* **2007**, *107*, 1831−1861. (g) Murphy, D. L.; Malachowski, M. R.; Campana, C.; Cohen, S. M. *Chem. Commun.* **2005**, 5506−5508. (h) Telfer, S. G.; Wuest, J. D. *Chem. Commun.* **2007**, 3166−3168. (i) Gupta, R. K.; Pandey, R.; Singh, R.; Srivastava, N.; Maiti, B.; Saha, S.; Li, P.; Xu, Q.; Pandey, D. S. *Inorg. Chem.* **2012**, *51*, 8916−8930. (j) Gupta, R. K.; Pandey, R.; Sharma, G.; Prasad, R.; Koch, B.; Srikrishna, S.; Li, Pei-Z.; Xu, Q.; Pandey, D. S. *Inorg. Chem.* **2013**, *52*, 3687−3698. (k) Gupta, R. K.; Sharma, G.; Pandey, R.; Kumar, A.; Koch, B.; Li, Pei-Z.; Xu, Q.; Pandey, D. S. *Inorg. Chem.* **2013**, *52*, 13984−13996. (l) Crawford, S. M.; Al-Sheikh, A. A.; Cameron, T. S.; Thompson, A. *Inorg. Chem.* **2011**, *50*, 8207−8213. (m) King, E. R.; Betley, T. A. *Inorg. Chem.* **2009**, *48*, 2361−2363. (n) King, E. R.; Hennessy, E. T.; Betley, T. A. *J. Am. Chem. Soc.* **2011**, *133*, 4917−4923. (o) Scharf, A. B.; Betley, T. A. *Inorg. Chem.* **2011**, *50*, 6837−6845. (p) Chisholm, M. H.; Choojun, K.; Gallucci, J. C.; Wambua, P. M. *Chem. Sci.* **2012**, *3*, 3445−3447. (q) King, E. R.; Sazama, G. T.; Betley, T. A. *J. Am. Chem. Soc.* **2012**, *134*, 17858−17861.
(10) (a) Ruffin, H.; Baudron, S. A.; Salazar-Mendoza, D.; Hosseini, M. W. *Chem.—Eur. J.* **2014**, *20*, 2449−2453. (b) Beziau, A.; Baudron, S. A.; Fluck, A.; Hosseini, M. W. *Inorg. Chem.* **2013**, *52*, 14439−14448. (c) Beziau, A.; Baudron, S. A.; Pogozhev, D.; Fluck, A.; Hosseini, M. W. *Chem. Commun.* **2012**, *48*, 10313−10315. (d) Beziau, A.; Baudron, S. A.; Hosseini, M. W. *Dalton Trans.* **2012**, *41*, 7227−7234. (e) Baudron, S. A. *CrystEngComm* **2010**, *12*, 2288−2295.
(11) (a) Yang, Y.; Ren, Y.; Sun, C.; Hao, S. *Green Chem.* **2014**, *16*, 2273−2280. (b) Lu, H.; Yin, H.; Liu, Y.; Jiang, T.; Yu, L. *Catal. Commun.* **2008**, *10*, 313−316. (c) Li, Pei-Zhou; Aijaz, A.; Xu, Q. *Angew. Chem., Int. Ed.* **2012**, *51*, 6753−6756.
(12) (a) Okubo, T.; Tanaka, N.; Kim, K. H.; Yone, H.; Maekawa, M.; Kuroda-Sowa, T. *Inorg. Chem.* **2010**, *49*, 3700−3702. (b) Okubo, T.; Anma, H.; Tanaka, N.; Himoto, K.; Seki, S.; Saeki, A.; Maekawa, M.; Kuroda-Sowa, T. *Chem. Commun.* **2013**, *49*, 4316−4318. (c) Wilton-Ely, J. D. E. T.; Solanki, D.; Knight, E. R.; Holt, K. B.; Thompson, A. L.; Hogarth, G. *Inorg. Chem.* **2008**, *47*, 9642−9653. (d) Heard, P. J. *Prog. Inorg. Chem.* **2005**, *53*, 1−69. (e) Tong, M. C.; Chen, W.; Sun, J.; Ghosh, D.; Chen, S. *J. Phys. Chem. B* **2006**, *110*, 19238−19242. (f) Cao, H.; Wei, M.; Chen, Z.; Huang, Y. *Analyst* **2013**, *138*, 2420−2426. (g) Vickers, M. S.; Cookson, J.; Beer, P. D.; Bishop, P. T.; Thiebaut, B. *J. Mater. Chem.* **2006**, *16*, 209−215.
(13) (a) Mayer, C. R.; Neveu, S.; Cabuil, V. *Angew. Chem., Int. Ed.* **2002**, *41*, 501−503. (b) Mayer, C. R.; Neveu, S.; Simonnet-Jegat, C.; Debiemme-Chouvy, C.; Cabuil, V.; Secheresse, F. *J. Mater. Chem.* **2003**, *13*, 338−341. (c) Nasr, G.; Guerlin, A.; Dumur, F.; Baudron, S. A.; Dumas, E.; Miomandre, F.; Clavier, G.; Sliwa, M.; Mayer, C. R. *J. Am. Chem. Soc.* **2011**, *133*, 6501−6504. (d) Mayer, C. R.; Dumas, E.; Miomandre, F.; Meallet-Renault, R.; Warmont, F.; Vigneron, J.; Pansu, R.; Etcheberry, A.; Secheresse, F. *New J. Chem.* **2006**, *30*, 1628−1637. (e) Mayer, C. R.; Dumas, E.; Secheresse, F. *J. Colloid Interface Sci.* **2008**, *328*, 452−457. (f) Miomandre, F.; Stancheva, S.; Audibert, J.-F.; Brosseau, A.; Pansu, R. B.; Lepeltier, M.; Mayer, C. R. *J. Phys. Chem. C* **2013**, *117*, 12806−12814. (g) Mayer, C. R.; Dumas, E.; Sécheresse, F. *Chem. Commun.* **2005**, 345−347.
(14) (a) Li, X.; Zhang, J.; Xu, W.; Jia, H.; Wang, X.; Yang, B.; Zhao, B.; Li, B.; Ozaki, Y. *Langmuir* **2003**, *19*, 4285−4290. (b) He, S.; Yao, J.; Jiang, P.; Shi, D.; Zhang, H.; Xie, S.; Pang, S.; Gao, H. *Langmuir* **2001**, *17*, 1571−1574. (c) Li, H.; Yao, Y.; Han, C.; Zhan, J. *Chem. Commun.* **2009**, 4812−4814.
(15) Perrin, D. D.; Armango, W. L. F.; Perrin, D. R. *Purification of Laboratory Chemicals;* Pergamon: Oxford, U.K., 1986.
(16) (a) Auger, A.; Swarts, J. C. *Organometallics* **2007**, *26*, 102−109. (b) Auger, A.; Muller, A. J.; Swarts, J. C. *Dalton Trans.* **2007**, 3623−3633. (c) Nemykin, V. N.; Galloni, P.; Floris, B.; Barrett, C. D.; Hadt, R. G.; Subbotin, R. I.; Marrani, A. G.; Zanoni, R.; Loim, N. M. *Dalton Trans.* **2008**, 4233−4246. (d) Gallagher, J. F.; Moriarty, E. *Acta Crystallogr., Sect. C* **1999**, *55*, 1079−1082.
(17) (a) Sheldrick, G. M. *SHELXL-97,* Program for X-ray Crystal Structure Refinement; Gottingen University: Gottingen, Germany, 1997. (b) Sheldrick, G. M. *SHELXS-97, Program for X-ray Crystal Structure Solution*; Gottingen University: Gottingen, Germany, 1997.
(18) (a) Spek, A. L. *PLATON,* A Multipurpose Crystallographic Tools; Utrecht University: Utrecht, The Netherlands, 2000. (b) Spek, A. L. *Acta Crystallogr., Sect. A* **1990**, *46*, C31−37.
(19) Becke, A. D. *J. Chem. Phys.* **1993**, *98*, 5648−5652.
(20) Lee, C. T.; Yang, W. T.; Parr, R. G. *Phys. Rev. B: Condens. Matter Mater. Phys.* **1988**, *37*, 785−789.
(21) Krishnan, R.; Binkley, J. S.; Seeger, R.; Pople, J. A. *J. Chem. Phys.* **1980**, *72*, 650−654.
(22) McClean, A. D.; Chandler, G. S. *J. Chem. Phys.* **1980**, *72*, 5639−5648.
(23) (a) Hay, P.; Wadt, W. R. *J. Chem. Phys.* **1985**, *82*, 270−283. (b) Wadt, W. R.; Hay, P. *J. Chem. Phys.* **1985**, *82*, 284−298.
(24) (a) Gryko, D.; Lindsey, J. S. *J. Org. Chem.* **2000**, *65*, 2249−2252. (b) Gao, G.; Korobkov, I.; Gambarotta, S. *Inorg. Chem.* **2004**, *43*, 1108−1115.
(25) (a) Birri, A.; Harvey, B.; Hogarth, G.; Subasi, E.; Ugur, F. *J. Organomet. Chem.* **2007**, *692*, 2448−2455. (b) Blake, A. J.; Kathirgamanathan, P.; Toohey, M. J. *Inorg. Chim. Acta* **2000**, *303*, 137−145.
(26) (a) Skibar, W.; Kopacka, H.; Wurst, K.; Salzmann, C.; Ongania, K. H.; Biani, F. F.; Zanello, P.; Bildstein, B. *Organometallics* **2004**, *23*, 1024−1041. (b) Malachowski, M. R.; Grau, M. F.; Thomas, J. M.; Rheingold, A. L.; Moore, C. E. *Inorg. Chim. Acta* **2010**, *364*, 132−137.
(27) (a) Pogozhev, D.; Baudron, S. A.; Hosseini, M. W. *CrystEngComm* **2010**, *12*, 2238−2244. (b) Gill, H. S.; Finger, I.; Bozidarevic, I.; Szydlo, F.; Scott, M. J. *New J. Chem.* **2005**, *29*, 68−71.
(28) (a) Husain, A.; Nami, S. A. A.; Singh, S. P.; Oves, M.; Siddiqi, K. S. *Polyhedron* **2011**, *30*, 33−40. (b) Harding, D. J.; Harding, P.; Dokmaisrijana, S.; Adams, H. *Dalton Trans.* **2011**, *40*, 1313−1321.
(29) Desiraju, G. R.; Steiner, T. *The Weak Hydrogen Bond in Structural Chemistry and Biology;* Oxford University Press: Oxford, U.K., 1999.
(30) Link, S.; El-Sayed, M. A. *J. Phys. Chem. B* **1999**, *103*, 4212−4217.
(31) Mie, G. *Ann. Phys.* **1908**, *25*, 377−455.
(32) (a) Lu, Y.; Mei, Y.; Drechsler, M.; Ballauff, M. *Angew. Chem., Int. Ed.* **2006**, *45*, 813−816. (b) Panigrahi, S.; Basu, S.; Praharaj, S.; Pande,

DOI: 10.1021/ic502848a
Inorg. Chem. 2015, 54, 2500−2511

S.; Jana, S.; Pal, A.; Ghosh, S. K.; Pal, T. *J. Phys. Chem. C* **2007**, *111*, 4596−4605.
(33) Baruah, B.; Gabriel, G. J.; Akbashev, M. J.; Booher, M. E. *Langmuir* **2013**, *29*, 4225−4234.
(34) (a) Chen, X.; Cai, Z.; Chen, X.; Oyama, M. *J. Mater. Chem. A* **2014**, *2*, 5668−5674. (b) Min, J.; Wang, F.; Cai, Y.; Liang, S.; Zhang, Z.; Jiang, X. *Chem. Commun.* **2014**, *51*, 761−764.

DOI: 10.1021/ic502848a
Inorg. Chem. 2015, 54, 2500−2511